Appl. Phys. A 78, 651–654 (2004)
DOI: 10.1007/s00339-003-2274-6

Applied Physics A
Materials Science & Processing

Ion beam assisted smoothing of optical surfaces

F. FROST✉
R. FECHNER
D. FLAMM
B. ZIBERI
W. FRANK
A. SCHINDLER

Leibniz-Institut für Oberflächenmodifizierung, Permoserstrasse 15, 04318 Leipzig, Germany

Received: 5 June 2003/Accepted: 18 June 2003
Published online: 12 November 2003 • **© Springer-Verlag 2003**

ABSTRACT In this work different ion-beam techniques demonstrate their capability for surface-roughness reduction down to the sub-nanometer scale. In ion beam direct smoothing, favorable characteristics in the development of surface topography are exploited and smoothing with the help of planarization layers is evaluated. Focusing on the common optical substrate materials quartz (fused silica) and silicon, it is shown that a surface-roughness reduction down to the ~ 0.1 nm root mean square level can be achieved by optimization and combination of these techniques.

PACS 78.67.-n; 61.46.+w; 68.37.Ps

1 Introduction

The surfaces roughness has a lasting effect on the mechanical, optical and electronic properties of numerous materials. Especially in the field of modern nanotechnology, permanently growing demands regarding nearly atomically smooth surfaces can be noted. Examples are X-ray optics, components for extreme-ultraviolet lithography as well as high-precision classical optics. Additionally, advanced applications of very thin films with thickness in the nanometer range require appropriate calibration standards. Substrates for such applications have to fulfill extremely high requirements concerning the surface roughness and flatness. Regarding the rms (root mean square) roughness as a measure of the deviation of the real surface from an ideally flat surface, rms values < 0.2 nm are commonly supposed for spatial wavelengths $< 1\,\mu$m (or $> 1\,\mu\text{m}^{-1}$ expressed in terms of spatial frequencies). Conventional polishing techniques are not qualified to meet this criterion. Therefore, alternative processes are necessary. Particularly, with regard to highly sophisticated finishing procedures for ultra-precise surface treatment, ion beam etching techniques become more and more a promising alternative for ultra-smooth surface manufacturing on the nanometer scale.

Basically, ion beam assisted smoothing can result from removing a planarized sacrificial layer as commonly used in semiconductor technology for the planarization of processed silicon wafers. For smoothing of optical surfaces this process was originally proposed by Johnson and Ingersoll [1] and further developed by Fechner et al. [2]. A second method is the direct ion bombardment of the surface at glancing incidence angles [3, 4], where surface asperities were removed by step-edge erosion. Recently, gas-cluster ion-beam processes were established as a further ion beam assisted smoothing technique [5, 6].

Beside these methods, smoothing of a wide variety of surface materials is also possible by ion-beam sputtering at normal or near-normal ion incidence as shown for semiconductors [7, 8] or thin diamond films [9, 10]. In this case different surface-smoothing mechanisms prevail over normally dominating roughening processes.

In this article ion beam direct smoothing at near-normal ion incidence and smoothing with planarization layers are evaluated. By optimization and combination of these techniques nanoscale surface smoothing down to sub-nanometer levels is demonstrated.

2 Experimental details

Ion-beam etching was performed in a custom-built ion beam etching system (base pressure of 1×10^{-6} mbar) using a Kaufman-type broad-beam ion source. Samples were mounted on a water-cooled substrate stage (temperature adjustable from 265 K to 370 K). All experiments were normally performed at room temperature, unless otherwise noted. Additionally, the sample stage can be rotated around the surface normal of the mounted sample and the angle of ion-beam incidence α_{ion} can be chosen in the range 0–90° with respect to the surface normal. The ion source used in the experiments was home-built, and the parameters were optimized with respect to well-defined ion-energy distributions and small ion-beam divergences [11, 12].

The surface topography was investigated by atomic force microscopy (AFM) using a NanoScope IIIa from Digital Instruments operating in tapping mode. All measurements were conducted in air using numerous silicon tips with a nominal tip radius of < 10 nm (as specified by the manufacturers). The AFM measurements were performed for different scan sizes with a resolution of 512×512 or 256×256 pixels. The rms surface roughness R_{q} was calculated using the

✉ Fax: +49-341/2352-595, E-mail: frank.frost@iom-leipzig.de

relation $R_q = \sqrt{\langle [h(\boldsymbol{r},t) - \langle h(\boldsymbol{r},t)\rangle]^2\rangle}$, where $\langle\rangle$ denotes the spatial average. Furthermore, the circularly averaged power spectral density as a second-order statistical parameter was calculated for roughness evaluation. Because a careful tip evaluation and calibration is important for a reliable roughness measurement a recently proposed special procedure was used to find high-quality Si tips from different manufacturers [13, 14]. Additionally, for a sound estimate of the systematic error caused by measurements with different tips two polished Si wafers (with a very uniform roughness across the whole wafer surface) were evaluated using 10 tips from the same manufacturer. The averaged rms roughness values for this procedure were determined as $R_q = (0.421 \pm 0.029)$ nm and $R_q = (0.151 \pm 0.015)$ nm, respectively. Therefore, a systematic error $< 10\%$ can be assumed for the measurements of the rms surface roughness.

The samples used in this work were commercially available quartz wafers (ultra-pure fused silica) and standard silicon wafers from different suppliers. The surfaces of these wafers were characterized by a rms roughness between 0.3 nm and 0.4 nm for the quartz wafers and < 0.2 nm for the Si wafers, respectively.

For planarization layers standard photoresist was spin coated onto the wafer surface using a commercial spin coater. The thickness of the photoresist layer varies between 90 and 110 nm.

3 Results and discussion

Besides the actual removal of material, the process of ion-beam erosion or sputtering often results in a pronounced topography evolution, generally accomplished by a kinetic roughening of the surface. In order to gain insight into the diversity of possible surface topographies caused by ion-beam erosion, four quartz surfaces are shown after 90 min of sputtering without (Fig. 1a and c) and with simultaneous sample rotation (Fig. 1b and d). The ion-beam angle of incidence was 50° for images (a) and (b), and 70° for images (c) and (d), respectively ($E_{ion} = 800$ eV, $j_{ion} = 400\,\mu A\,cm^{-2}$). For fixed azimuthal directions of the impinged ion beam (no rotation) the surface consists of ripple-like structures. This phenomenon is a prominent example of self-organization during ion sputtering. Due to the rotation of the sample the surface structures no longer show a preferred orientation. There are also striking differences between surfaces (b) and (d). While the surface eroded at 50° is extremely smooth ($R_q \approx 0.1$ nm) and unstructured, the surface sputtered at 70° shows a random roughness consisting of hillocks and hillock clusters with different sizes. Generally, ion-beam erosion of quartz leads to either a smooth surface below and salient surface features above a critical ion incidence angle. For further details concerning the ion-beam erosion of quartz the reader is referred to former work [15, 16].

In regard to surface smoothing, it interesting that for ion incidence angles $\leq 50°$ extremely smooth surfaces are obtained, offering a direct surface-smoothing effect by the ion beam. Utilizing ion-beam sputtering under nearly identical conditions on rough surfaces results in a pronounced roughness reduction. This is illustrated in Fig. 2, where the surface of an as-received quartz wafer was considerably smoothed under optimized ion beam sputter conditions down to ≤ 0.1 nm. From Fig. 3 it is evident that smoothing occurs over all spatial frequencies covered by the AFM measurements. Similar smoothing effects are observed for many different material/ion combinations under suitable conditions. Former work was targeted to different compound semiconductor materials, which were smoothed by low-energy N_2^+-ion beams, emphasizing the importance of the ion species used in ion-beam sputtering [7, 8].

In contrast to ion-beam erosion of quartz the topography development of Si during Ar^+-ion-beam sputtering bears a very complex behavior. For near-normal ion incidence angles and ion energy ≤ 700 eV the surface exhibits a network of hole-like structures which coarsen with etch time (see Fig. 4d). Similar surface topographies were observed in plasma etching of Si [17, 18]. However, at more oblique ion incidence angles between 35° and 60°, smooth surfaces with rms roughness ≤ 0.2 nm are obtained. Further increasing of the ion incidence angle results in fine dot structures on the whole surface (see Fig. 4a). Detailed investigations are currently in progress and will be published elsewhere. Never-

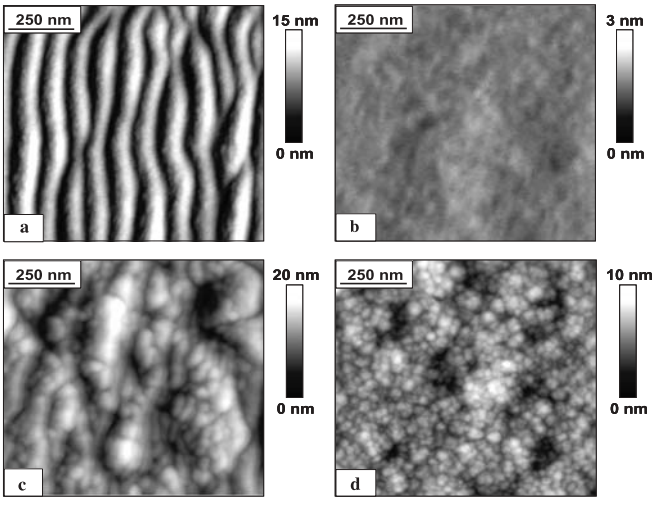

FIGURE 1 Topography of a quartz surface after Ar^+ sputtering (ion energy 800 eV, ion current density 400 $\mu A\,cm^{-2}$) without [(**a**) and (**c**)] and with simultaneous sample rotation [(**b**) and (**d**)]. The ion-beam angle of incidence was 50° for images (**a**) and (**b**) and 70° for images (**c**) and (**d**). The images were taken after a sputter times of 90 min. All AFM images show a surface area of 1 $\mu m \times 1$ μm. Please note the different height scales for the individual images

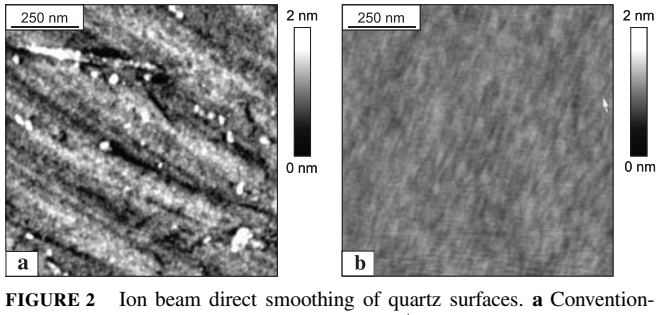

FIGURE 2 Ion beam direct smoothing of quartz surfaces. **a** Conventionally polished surface (as received), **b** after Ar^+-ion-beam direct smoothing (sample rotation, ion energy 800 eV, ion current density 400 $\mu A\,cm^{-2}$, ion incidence angle 20°, sputter time 20 min)

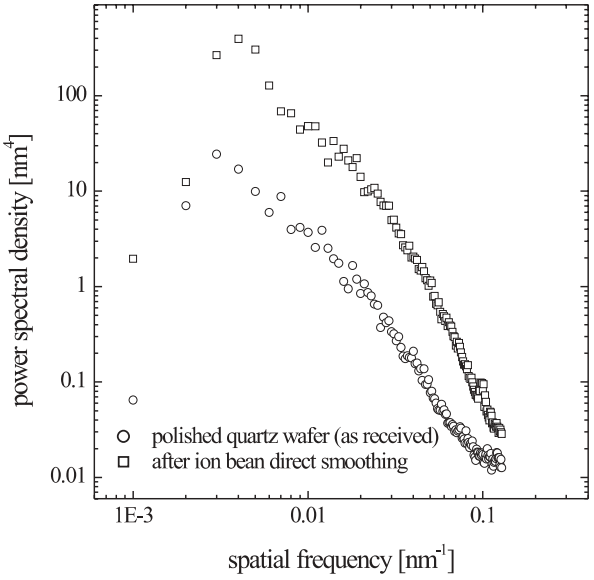

FIGURE 3 Circularly averaged power spectral density for the surfaces shown in Fig. 2. Surface smoothing for all spatial wavelengths is evident

theless, from this presentation it is clear that conditions exist where surface smoothing can be expected. Scrutinizing this possibility, a Si wafer surface was consciously roughened under unfavorable sputter conditions whereby holes as well as dot structures are generated (see Fig. 4a and d). Subsequently, both surfaces were ion beam smoothed under suitable conditions (ion energy 500 eV, incidence angle 40°, sputter time 10 min). Representative AFM snapshots taken from these surfaces are shown in Fig. 4b and e. Even though both initial surfaces were characterized by nearly the same rms roughness (dot-like structured surface: $R_q \sim 2.1$ nm; hole-like structured surface: $R_q \sim 1.7$ nm) the degree of roughness reduction by ion-beam smoothing is rather different for both surfaces. While the small dot-like asperities from Fig. 4a completely disappeared in Fig. 4b the hole-like depressions are still obvious (Fig. 4d and e). This is also confirmed by rms values of $R_q \sim 0.4$ nm and $R_q \sim 1.1$ nm for the surfaces shown in Fig. 4b and e. The reason for this different smoothing behavior are the various portions of high spatial frequency and low spatial frequency surface wavelengths that determine the efficiency of the ion beam smoothing process. Surface irregularities with high spatial frequencies are smoothed out rapidly, while low spatial frequency components require longer sputter times. In Fig. 5 the time dependence of the ion beam direct smoothing is summarized. An almost exponential decrease of R_q with proceeding etch time or ion dose was observed. This smoothing kinetics can be understood within the framework of a linear theory for the topography development during sputtering, assuming that different surface-relaxation mechanisms prevail over roughening processes [19]. Figure 5 also substantiates the enhanced smoothing efficiency of high spatial frequency roughness components. However, it should be noted that for both surfaces a final-state rms roughness below 0.2 nm is obtained, which is equivalent to the rms value after long-time sputtering of an unprocessed initially smooth wafer.

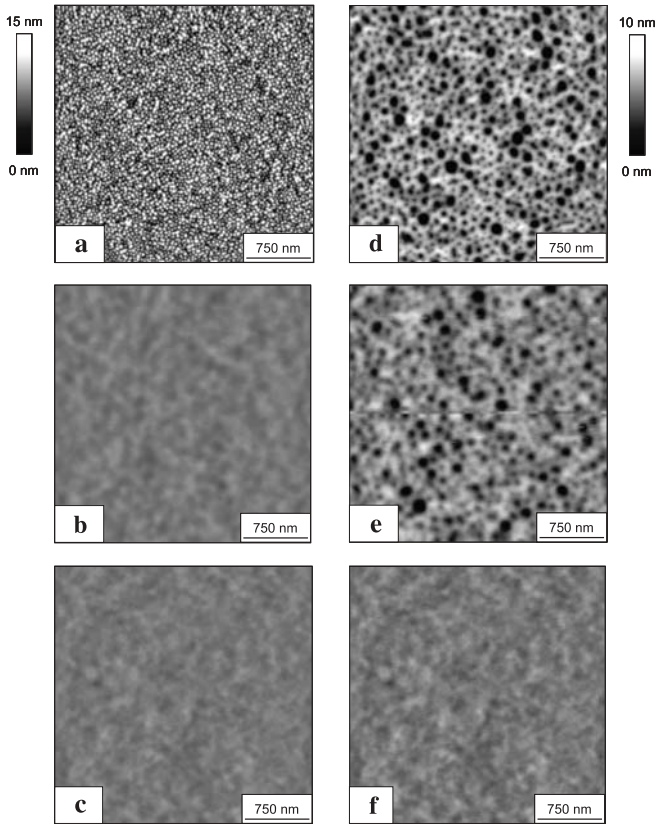

FIGURE 4 Silicon surface topographies before and after smoothing. Surfaces **a** and **d** were pre-roughened by Ar^+-ion-beam etching (sample rotation, ion energy 500 eV, ion current density 300 μA cm^{-2}, sputter time 20 min) at ion incidence angles of 0° and 75°, respectively. Images **b** and **e** show surfaces **a** and **d** after ion beam direct smoothing (ion energy 500 eV, incidence angle 40°, sputter time 10 min). Images **c** and **f** are obtained from surfaces **a** and **d** after planarization utilizing photoresist as planarization layer (ion energy 500 eV, incidence angle 45°, over-etching time 10 min)

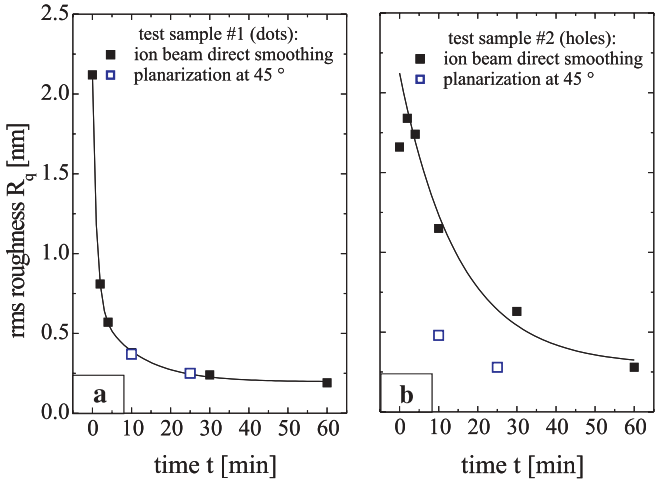

FIGURE 5 Kinetics of ion beam direct smoothing for two test samples (no. 1: dot-like structured surface corresponding to Fig. 4a, no. 2: hole-like structured surface corresponding to Fig. 4d). For comparison the rms roughness values of Si surfaces obtained by planarization followed by 10- and 25-min ion-beam etching are also displayed

To speed up the roughness reduction and shorten the process time the planarization technique was tested. After coating our Si model surfaces (Fig. 4a and d) with photoresist to level out the surface roughness the resist was removed by Ar^+-ion-

beam sputtering under an ion incidence angle of 45°. Under these conditions the removal rates of the resist and the underlying Si surface are nearly identical. Thus the smooth resist surface is transferred into the Si surface [20]. After removal of the resist the uncovered Si surface was sputtered for another 10 min (over-etching) to promote the effect of ion beam direct smoothing. The resulting topographies are given in Fig. 4c and f. The rms roughness was measured as $R_q \sim 0.4$ nm and $R_q \sim 0.5$ nm for the surfaces shown in Fig. 4c and f, respectively. Whereas the roughness obtained for the dot-like structured surface is comparable to ion beam direct smoothing, the roughness for the hole-like structured surface was significantly improved compared to ion beam direct smoothing. This result is attributed to the enhanced decrease of the low spatial frequency surface wavelength. For comparison with ion beam direct smoothing the rms roughness values obtained by planarization after 10- and 25-min Si ion beam etching are also displayed in Fig. 5. Considering the dot-like Si model surface both processes, ion beam direct smoothing and the planarization technique, are equivalent. However, for the hole-like Si model surface containing more low spatial frequency surface-wavelength structures, an additional planarization step is essential.

4 Conclusions

Surface smoothing using low-energy ion beams was shown for common optical substrate materials. Especially, ion beam direct smoothing and smoothing with planarization layers are investigated. The combination of both these techniques offers sub-nanometer scale roughness reduction down to ~ 0.1 nm rms covering a broad range of spatial frequency surface-wavelength structures. Due to the application of broad-beam ion sources the results are also applicable to large-scale optical surfaces. Currently the ongoing work is extended to ion-assisted surface smoothing of other relevant materials like SiC as well as different glass ceramics developed for mask substrates for future extreme-ultraviolet lithography.

ACKNOWLEDGEMENTS This work is supported by the Deutsche Forschungsgemeinschaft (Grant Nos. FOR 365/1-1 and 2).

REFERENCES

1 L.F. Johnson, K.A. Ingersoll: Appl. Opt. **22**, 1165 (1983)
2 R. Fechner, A. Schindler, T. Hänsel, F. Bigl: *Precision Science and Technology for Perfect Surfaces*, ed. by Y. Furukawa, Y. Mori, T. Kataoka (The Japan Society for Precision Engineering, Tokyo 1999) p. 249
3 M. Wißing, M. Batzill, K.J. Snowdon: Nanotechnology **8**, 40 (1997)
4 K. Kimura, A. Fukui, K. Nakajima, M.H. Mannami: Nucl. Instrum. Methods B **148**, 149 (1999)
5 L.P. Allen, D.B. Fenner, V. DiFilippo, C. Santeufemio, E. Degenkolb, W. Brooks, M. Mack, J. Hautala: J. Electron. Mater. **30**, 829 (2001)
6 D.B. Fenner, V. DiFilippo, J.A. Bennett, T.G. Tetreault, J.K. Hirvonen, L.C. Feldman: Proc. SPIE **4468**, 17 (2001)
7 F. Frost, A. Schindler, F. Bigl: Appl. Phys. A **66**, 663 (1998)
8 F. Frost, G. Lippold, K. Otte, D. Hirsch, A. Schindler, F. Bigl: J. Vac. Sci. Technol. A **17**, 793 (1999)
9 A. Hirata, H. Tokura, M. Yoshikawa: Thin Solid Films **212**, 43 (1992)
10 S. Kiyohara, I. Miyamoto, T. Masaki, S. Honda: Nucl. Instrum. Methods B **121**, 191 (1997)
11 M. Zeuner, J. Meichsner, H. Neumann, F. Scholze, F. Bigl: J. Appl. Phys. **80**, 611 (1996)
12 M. Tartz, E. Hartmann, F. Scholze, H. Neumann: Rev. Sci. Instrum. **69**, 1147 (1998)
13 F. Frost, D. Hirsch, A. Schindler: Appl. Surf. Sci. **179**, 8 (2001)
14 F. Frost, D. Hirsch, A. Schindler, B. Rauschenbach: Proc. SPIE **4449**, 225 (2001)
15 D. Flamm, F. Frost, D. Hirsch: Appl. Surf. Sci. **179**, 95 (2001)
16 F. Frost, D. Flamm: submitted
17 Y.-P. Zhao, J.T. Drotar, G.-C. Wang, T.-M. Lu: Phys. Rev. Lett. **82**, 4882 (1999)
18 J.T. Drotar, Y.-P. Zhao, T.-M. Lu, G.-C. Wang: Phys. Rev. B **61**, 3012 (2000)
19 E. Chason, T.M. Mayer, B.K. Kellerman, D.T. McIlroy, A.J. Howard: Phys. Rev. Lett. **72**, 3040 (1994)
20 For further description and details of the planarization technique, the reader is referred to [2]